Supporting Information

Comparing Rate and Mechanism of Ethane Hydrogenolysis on Transition Metal Catalysts

Abdulrahman Almithn and David Hibbitts*
Department of Chemical Engineering, University of Florida, Gainesville, Florida, 32611, United States
*Corresponding author: hibbitts@che.ufl.edu

Table of Contents

List of Tables

List of Figures

S1. Details of Density Functional Calculations of Thermochemical Properties

Frequency calculations were performed on gas phase molecules and all optimized adsorbed species to determine zero-point vibrational energies (ZPVE), and vibrational, translational and rotational enthalpy and free energy. These terms were then used, together with electronic energies (E_0, provided by VASP), to estimate enthalpies (*H*)

$$H = E_0 + \mathrm{ZPVE} + H_{\mathrm{vib}} + H_{\mathrm{trans}} + H_{\mathrm{rot}} \quad \text{(S1)}$$

and free energies (*G*)

$$G = E_0 + \mathrm{ZPVE} + G_{\mathrm{vib}} + G_{\mathrm{trans}} + G_{\mathrm{rot}} \quad \text{(S2)}$$

for reactants, products, and transition states at 593 K (the temperature at which ethane hydrogenolysis rates were measured). The entropy can be determined for a state with a known *H* and *G* at a given *T*:

$$S = \frac{H - G}{T} \quad \text{(S3)}$$

For calculations which include a periodic metal surface or a metal half-particle, the translational and rotational degrees of freedom are hindered and treated as vibrations. DFT-derived vibrational frequencies can then be used to determine the ZPVE, H_{vib}, and G_{vib}

$$ZPVE = \sum_i (½ \nu_i h) \quad \text{(S4)}$$

$$H_{vib} = \sum_i \left(\frac{\nu_i h e^{\frac{-\nu_i h}{kT}}}{1 - e^{\frac{-\nu_i h}{kT}}} \right) \quad \text{(S5)}$$

$$G_{vib} = \sum_i \left(-kT \ln \frac{1}{1 - e^{\frac{-\nu_i h}{kT}}} \right) \quad \text{(S6)}$$

For gaseous molecules, translational and rotational enthalpies and free energies were also computed from statistical mechanics:

$$H_{trans} = \frac{5}{2} kT \quad \text{(S7)}$$

$$H_{rot,linear} = kT \quad \text{(S8)}$$

$$H_{rot,nonlinear} = \frac{3}{2} kT \quad \text{(S9)}$$

$$G_{trans} = -kT \ln\left[\left(\frac{2\pi MkT}{h^2} \right)^{3/2} V \right] \quad \text{(S10)}$$

$$G_{rot} = -kT \ln\left[\frac{\pi^{1/2}}{\sigma} \left(\frac{T^3}{\theta_x \theta_y \theta_z} \right)^{1/2} \right] \quad \text{(S11)}$$

$$\theta_i = \frac{h^2}{8\pi^2 I_i k} \quad \text{(S12)}$$

where I_i is the moment of inertia about axes *x*, *y* or *z* and σ is the symmetry number of the molecule (2 for H_2 and 6 for C_2H_6). Equations S7–S12 obtained from: McQuarrie, D. A.; Statistical Mechanics; Sausolito, CA.

S2. Entropy of adsorbed H adjustments*

H* is known to saturate Pt and other transition metals surfaces at alkane hydrogenolysis conditions and even at ambient conditions during H_2 chemisorption measurements, leading to coverages of ≥ 1 ML.[37,81,89–91] However, the entropies of adsorbed species, such as H* (S[H*]), are often underestimated using traditional harmonic oscillator approximations and vibrational frequency analysis performed by DFT, leading to inaccurate estimates of desorption free energies (ΔG_γ). For example, the DFT-predicted S[H*] value is ~ 15 J mol^{-1} K^{-1} at 593 K on Pt (Table S1), far below measured values during high-temperature chemisorption experiments (~ 60 J mol K^{-1}) and values predicted by quantum and semi-classical treatments of a DFT-generated PES on Pt(100).[58] Unadjusted S[H*] values would give negative ΔG_γ values that become more negative with decreasing H* coverage at 593 K (Table S1), indicating favorable desorption which is inconsistent with high H* coverages at hydrogenolysis conditions. These findings indicate that S[H*] values, predicted by immobile adsorption models, are unreliable and must be corrected. Therefore, S[H*] values on Pt(111) were multiplied by a factor ~ 4 to give an average value near 60 J mol K^{-1} (the experimentally measured value at 593). The adjusted ΔG_γ values are positive and increase with decreasing the H* coverage, consistent with high H* coverages at hydrogenolysis conditions (Table S1). Similar adjustments have been made for all other metals (Table S1) and for the Pt_{119} half-particle (Tables S2 and S3).

Table S1. DFT-predicted energies to desorb γ H* before and after adjustment (593 K).

Catalyst	γ	ΔH_γ kJ mol^{-1}	ΔG_γ kJ mol^{-1}	S[H*] J mol^{-1} K^{-1} H*$^{-1}$	S[H*]$_{adjusted}$ J mol^{-1} K^{-1} H*$^{-1}$	$\Delta G_{\gamma,adjusted}$ kJ mol^{-1}
3×3 Ru(001)	1	27	−13	8	34	3
	2	57	−23	7	33	7
	3	91	−28	8	36	22
	4	128	−31	8	37	38
	8	294	−20	9	41	131
	9	340	−12	9	42	160
3×3 Os(001)	1	13	−25	12	52	0
	2	29	−46	12	53	2
	3	48	−65	12	52	7
	4	67	−84	11	51	11
	8	188	−114	12	52	77
	9	226	−114	12	52	101
3×3 Rh(111)	1	28	−11	9	39	6
	2	57	−21	9	40	16
	3	88	−30	9	40	26
	4	120	−37	9	41	39
	8	255	−55	10	44	108
	9	291	−57	10	45	131
3×3 Ir(111)	1	17	−20	12	55	5
	2	32	−41	13	58	12
	3	49	−62	13	58	18
	4	70	−77	13	60	33
	8	155	−132	15	66	111
	9	181	−141	15	68	140
3×3 Ni(111)	1	31	−11	5	21	0
	2	62	−21	5	24	1
	3	95	−29	5	25	5
	4	130	−35	6	27	15
	8	272	−52	7	31	64
	9	310	−53	7	33	82
3×3 Pd(111)	1	26	−13	9	40	5
	2	53	−27	8	37	7
	3	78	−41	8	37	10
	4	108	−50	9	39	22
	8	247	−66	9	42	88
	9	289	−62	9	42	114
3×3 Pt(111)	1	10	−26	14	63	3
	2	21	−52	14	62	6
	3	36	−74	14	62	12
	4	51	−93	14	65	28
	8	132	−151	16	70	108
	9	160	−156	16	72	141

Table S2. DFT-predicted energies to desorb γ H* before and after adjustment (593 K) on Pt_{119}.

Catalyst	γ	ΔH_γ kJ mol^{-1}	ΔG_γ kJ mol^{-1}	S[H*] J mol^{-1} K^{-1} H*$^{-1}$	S[H*]$_{adjusted}$ J mol^{-1} K^{-1} H*$^{-1}$	$\Delta H_{\gamma,adjusted}$ kJ mol^{-1}	$\Delta G_{\gamma,adjusted}$ kJ mol^{-1}
Pt_{119}	1	6	−31	15	65	15	9
	2	15	−56	15	65	34	23
	3	24	−83	15	65	53	36
	4	38	−101	15	65	77	56
	5	48	−127	15	65	97	70
	10	127	−222	15	65	223	172
	19	407	−273	16	66	590	476

Table S3. DFT-predicted energies to desorb γ H* before and after adjustment (300 K) on Pt_{119}.

Catalyst	γ	ΔH_γ kJ mol^{-1}	ΔG_γ kJ mol^{-1}	S[H*] J mol^{-1} K^{-1} H*$^{-1}$	S[H*]$_{adjusted}$ J mol^{-1} K^{-1} H*$^{-1}$	$\Delta H_{\gamma,adjusted}$ kJ mol^{-1}	$\Delta G_{\gamma,adjusted}$ kJ mol^{-1}
Pt_{119}	1	5	−13	6	56	15	12
	2	15	−21	6	56	34	29
	3	23	−30	6	56	52	44
	4	37	−32	6	56	76	66
	5	48	−40	6	56	96	83
	10	125	−50	6	56	221	197
	19	402	−63	8	58	586	532

S3. DFT-predicted reaction enthalpy diagrams

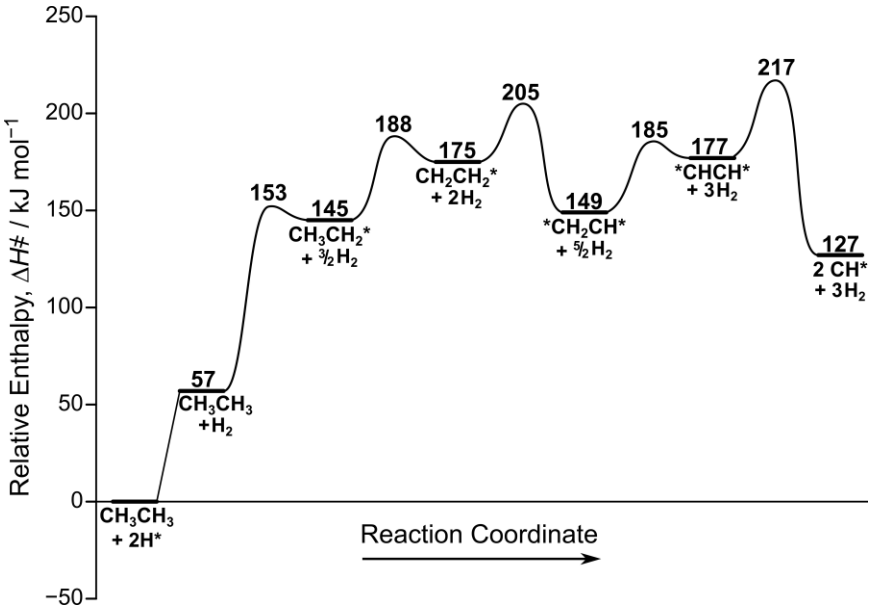

Figure S1. DFT-predicted reaction enthalpy diagram for ethane hydrogenolysis on a Ru(001) surface at 593 K.

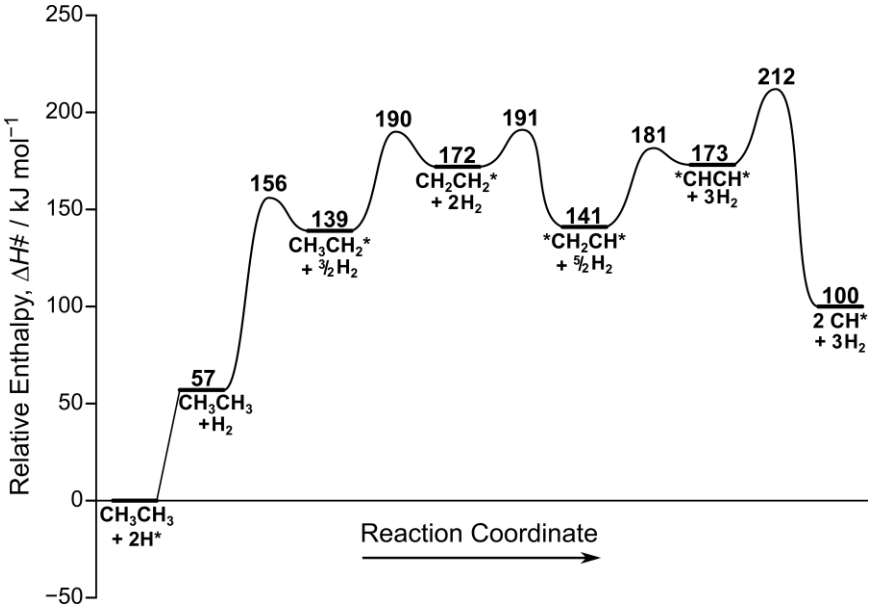

Figure S2. DFT-predicted reaction enthalpy diagram for ethane hydrogenolysis on a Os(001) surface at 593 K.

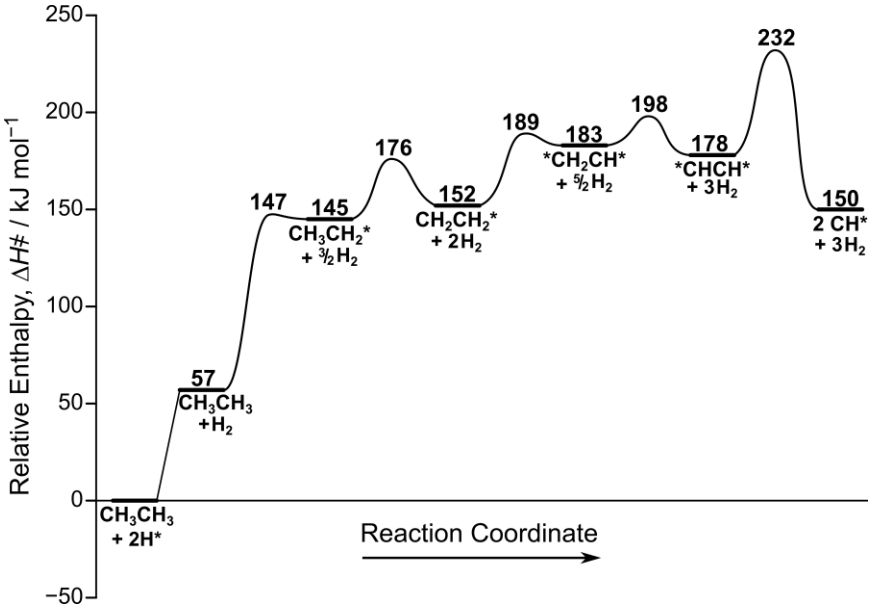

Figure S3. DFT-predicted reaction enthalpy diagram for ethane hydrogenolysis on a Rh(111) surface at 593 K.

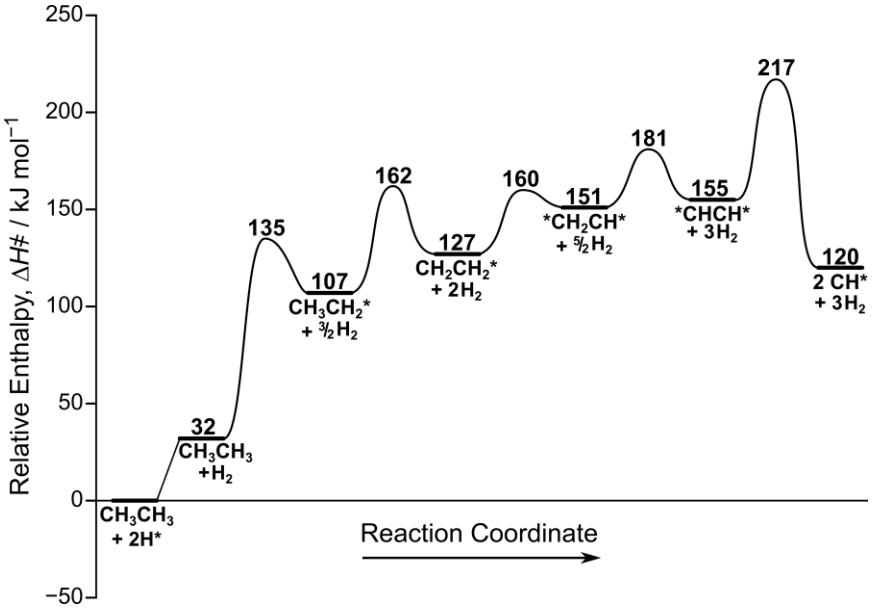

Figure S4. DFT-predicted reaction enthalpy diagram for ethane hydrogenolysis on a Ir(111) surface at 593 K.

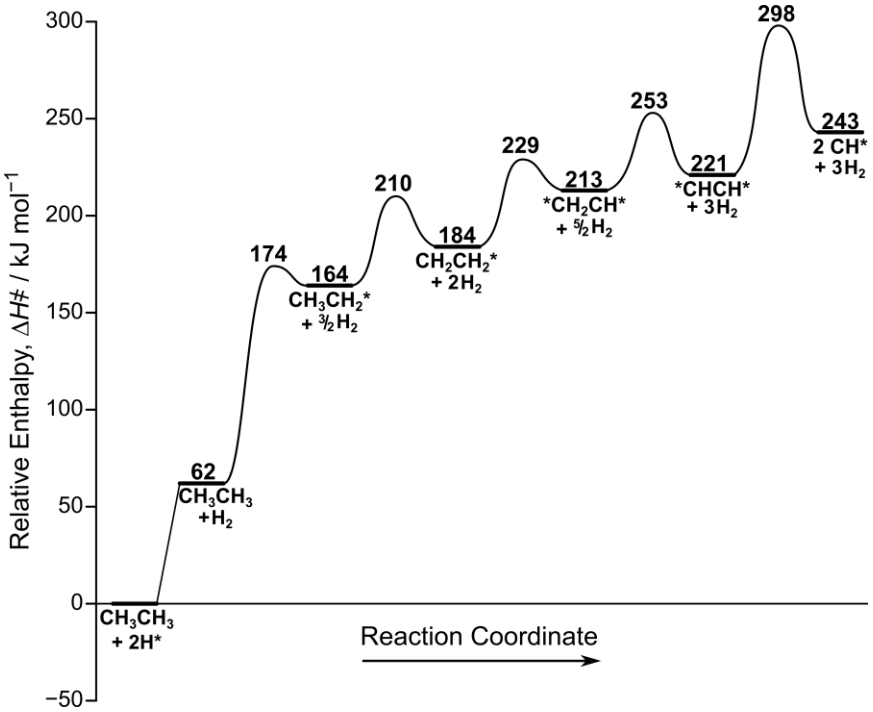

Figure S5. DFT-predicted reaction enthalpy diagram for ethane hydrogenolysis on a Ni(111) surface at 593 K.

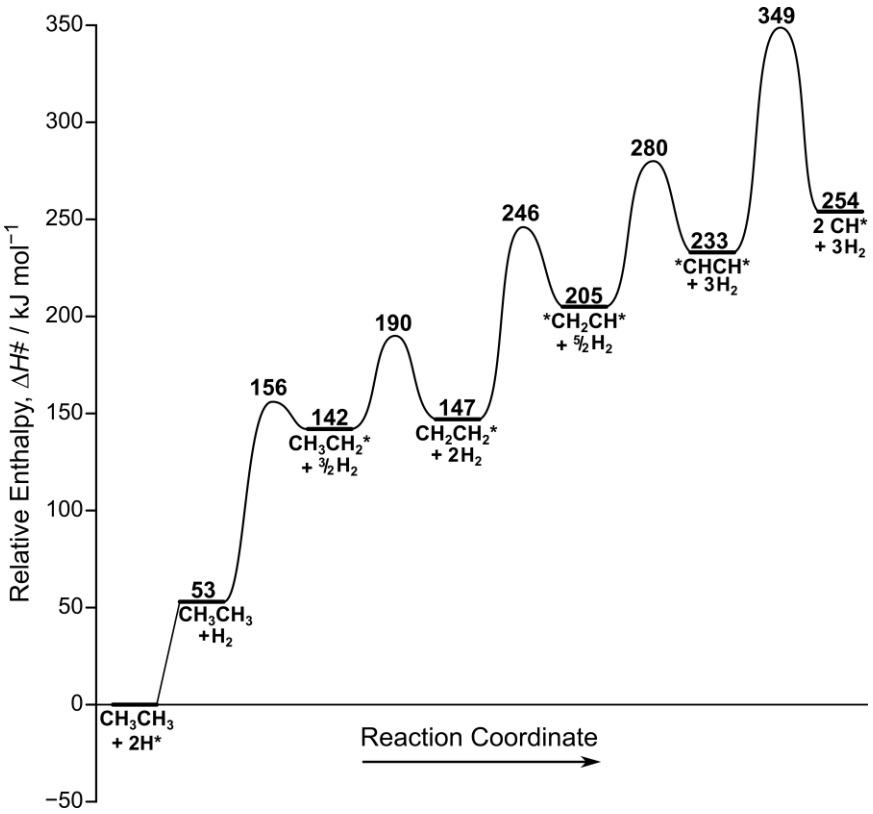

Figure S6. DFT-predicted reaction enthalpy diagram for ethane hydrogenolysis on a Pd(111) surface at 593 K.

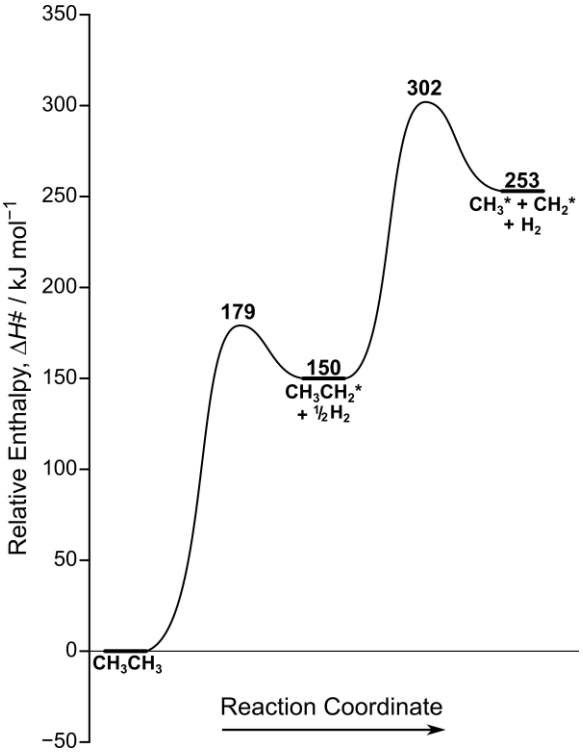

Figure S7. DFT-predicted reaction enthalpy diagram for ethane hydrogenolysis on a Cu(111) surface at 593 K.

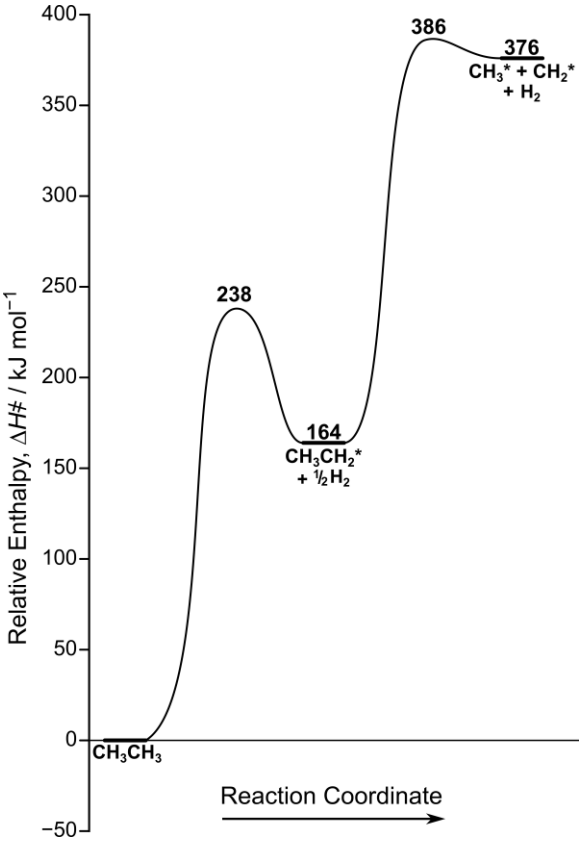

Figure S8. DFT-predicted reaction enthalpy diagram for ethane hydrogenolysis on a Ag(111) surface at 593 K.

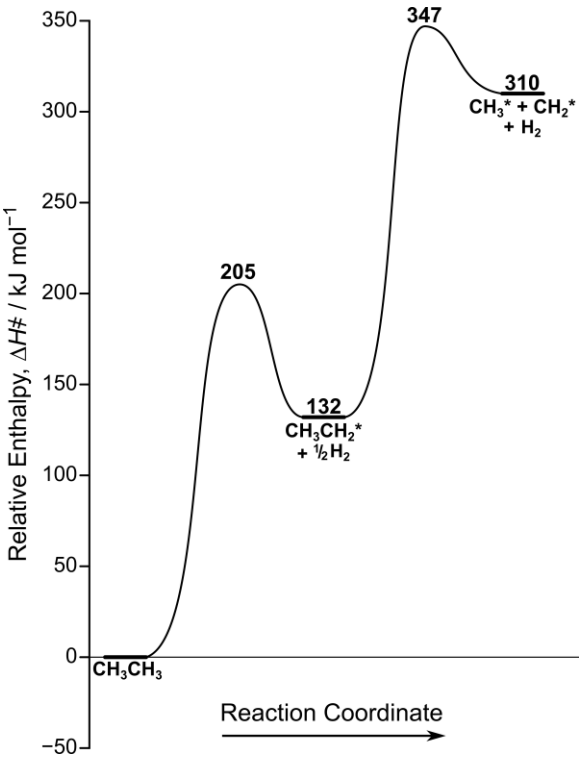

Figure S9. DFT-predicted reaction enthalpy diagram for ethane hydrogenolysis on a Au(111) surface at 593 K.

S4. DFT-predicted turnover rates for C–C bond cleavage in each intermediate

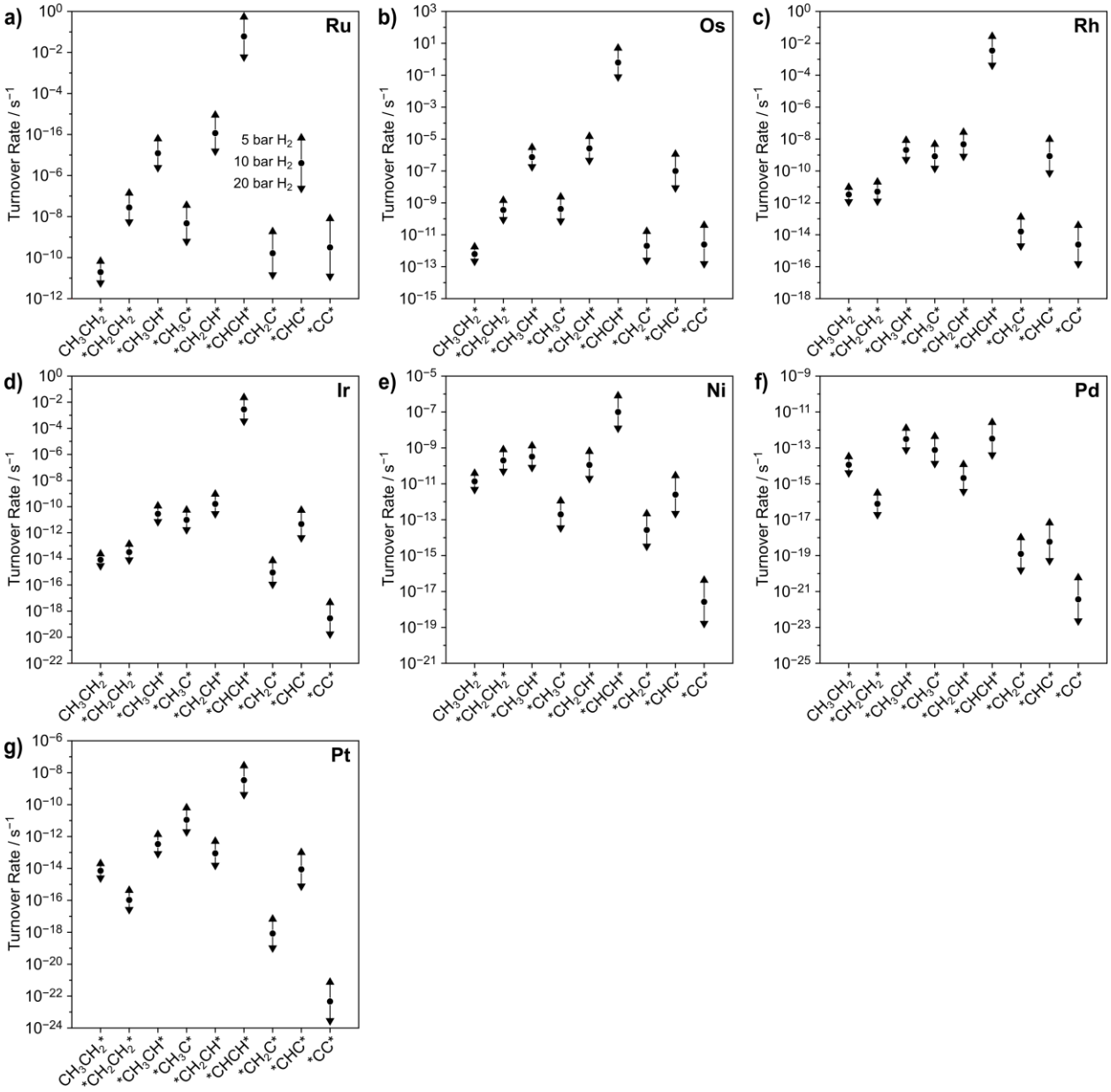

Figure S10. DFT-predicted turnover rates for C–C bond cleavage in each intermediate calculated using Equation 4 (593 K, 0.2 bar C_2H_6, 10 bar H_2) on a) Ru(001), b) Os(001), c) Rh(111), d) Ir(111), e) Ni(111), f) Pd(111), and Pt(111) surfaces. Up/down arrows represent 5 and 20 bar H_2, respectively.